CFD Modeling of Bubble Column Reactor Including the Influence of Gas Contraction

By *J. M. van Baten* and *R. Krishna**

In this paper a CFD model for a bubble column reactor undergoing a first order reaction A → B is developed. The reactor operates in the homogeneous bubbly regime and has a diameter D_T = 1 m and height H_T = 5 m. The incoming gas stream contains inerts, varying in proportion from 10 % to 90 %. Three-dimensional transient Eulerian simulations were carried out for an inlet superficial gas velocity U_G = 0.04 m/s. Due to the consumption of A, the gas phase suffers contraction along the height of the reactor and as a consequence there is a significant change in the gas velocity along the column height; this variation in gas velocity is stronger when the incoming gas contains a smaller proportion of inerts. The CFD simulations show that there is a considerable influence of gas contraction on both the bubble column hydrodynamics and on the reactor conversion. None of the conventionally used reactor models is capable of describing the reactor performance in the case of high gas phase contraction.

1 Introduction

In many examples of industrial importance a bubble column reactor is used to convert a reactant in the gas phase, A, to a valuable product, B, in the liquid phase by either homogeneously or heterogeneously catalysed reaction A → B. If the incoming gas stream contains a large proportion of inert, non-reactive components, there is only a small reduction in the superficial gas velocity U_G, along the reactor height. However, if the incoming gas stream contains a very small proportion of inerts then there is a significant reduction in U_G, especially when high conversion levels are aimed for. Consider for example the industrially important Fischer-Tropsch process for converting syngas (A), a mixture of CO and H_2, into long chain paraffinic hydrocarbons (B). At desired syngas conversion levels of 95 % there is a 60 – 70 % reduction in U_G from inlet to outlet of the bubble column slurry reactor [1]. The variation of U_G along the reactor height can be expected to have a significant influence on the hydrodynamics (gas holdup, backmixing) and mass transfer and, consequently also on the reactor conversion [1–3]. Most experimental studies on bubble column hydrodynamics are carried out in cold-flow experimental setups wherein no chemical reaction takes place and in which the variation of U_G along the reactor height is only due to hydrostatic pressure changes [4–8]. The correlations for gas holdup, backmixing, and mass transfer derived in such experimental studies cannot be used with complete confidence for scaling up a bubble column slurry reactor say for Fischer Tropsch synthesis designed for high syngas conversions.

Several recent publications have established the potential of Computational Fluid Dynamics (CFD) in the Eulerian framework for describing the hydrodynamics of bubble columns [9–18]. These CFD models, developed for either the homogeneous or heterogeneous flow regimes, are particularly suitable for describing scale effects [18,19]. However, it has been pointed out in recent works that the hydrodynamics and mass transfer characteristics of columns larger than say 1 m in diameter, can only be captured properly by three-dimensional transient simulations [20,21] that adequately portray the true chaotic behavior. In principle, CFD models offer a consistent physical basis for also accounting for the influence of varying U_G on hydrodynamics and the objective of the present work is to develop such a CFD model. We consider a first order reaction A → B in the liquid phase. The present work is an extension of the approach we have published earlier for the case without gas contraction [22]. The influence of gas contraction is investigated by allowing the incoming gas stream to contain varying proportion of non-reactive inert components. We restrict our model development to the homogeneous bubbly flow regime of operation.

2 Development of a CFD Model

Simulations were carried out for a column of diameter D_T = 1m and height H_T = 5 m with co-current up-flow of gas and liquid phases (see Fig. 1). The number of grid cells in the radial, axial and azimuthal directions are 50, 250, and 10, respectively, yielding a total of 125000 grid cells. In all the simulations, the superficial liquid velocity U_{L0} (=U_L) at the bottom inlet was maintained at 0.001 m/s. The superficial gas velocity U_{G0} at the bottom inlet was kept constant at 0.04 m/s. Varying proportion of inerts, 10 %, 30 %, 50 %, and 90 % were assumed for the incoming gas stream. The flow rate of reactant A in the inlet gas stream was kept constant for all of the four runs, and therefore the inlet gas concentration c_{AG0} varies with the proportion of inert gas present in the incoming gas. The physical and transport properties of

[*] J. M. van Baten, R. Krishna (R.Krishna@uva.nl), Van 't Hoff Institute for Molecular Sciences, University of Amsterdam, Nieuwe Achtergracht 166, 1018 WV Amsterdam, The Netherlands.

  DOI: 10.1002/ceat.200407018 *Chem. Eng. Technol.* **2004**, *27*, No. 12

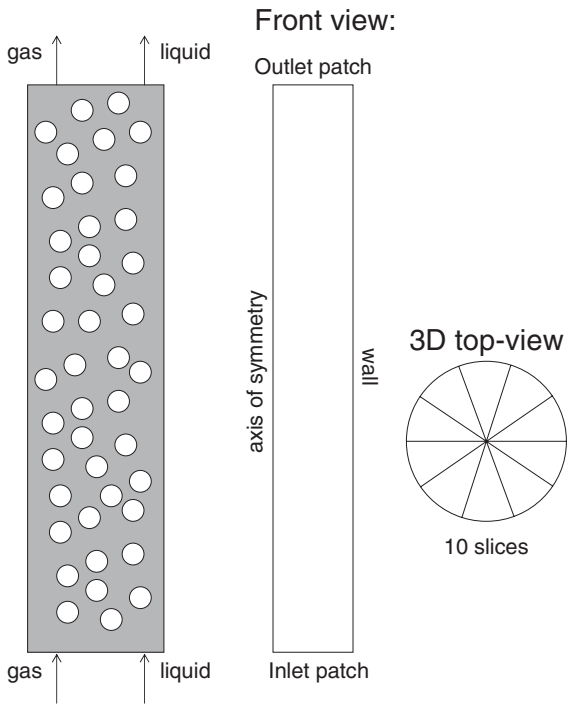

Figure 1. Schematic overview of the computational domains, including front and top views.

the gas and liquid phases are specified in Tab. 1. In each case two different types of simulations were carried out:

1) Determination of the quasi-steady state *hydrodynamics*.
2) Determination of the conversion for the liquid phase *reaction* A → B, with the reactant A introduced into the reactor via the gas inlet. The component B was assumed to be present only in the liquid phase.

We discuss the modeling of the two steps, in turn.

Table 1. Properties used in the CFD simulations.

	Liquid (water)	Gas (air)
Viscosity, μ / [Pa s]	$1{\cdot}10^{-3}$	$1.7{\cdot}10^{-5}$
Diffusivity of component, $Đ$ / [m^2 s^{-1}]	$1{\cdot}10^{-9}$	$1.0{\cdot}10^{-5}$
Density, ρ / [kg/m^3]	998	1.3
Interphase mass transfer coefficient, k_L / [m/s]	0.0004	
Reaction rate constant, k_A / [s^{-1}]	0.2	
Henry coefficient, m / [–]	0.3	

2.1 CFD Modeling of Bubble Column Hydrodynamics

For either the fluid phase in the bubble column reactor, the volume-averaged mass and the momentum conservation equations in the Eulerian framework are given by[1)]:

$$\frac{\partial\left(\varepsilon_k\rho_k\right)}{\partial t}+\nabla\bullet\left(\rho_k\varepsilon_k\mathbf{u}_k\right)=0 \tag{1}$$

$$\frac{\partial\left(\rho_k\varepsilon_k\mathbf{u}_k\right)}{\partial t}+\nabla\bullet\left(\rho_k\varepsilon_k\mathbf{u}_k\mathbf{u}_k\right)=\mu_{k,eff}\,\varepsilon_k\left(\nabla\mathbf{u}_k+\left(\nabla\mathbf{u}_k\right)^{\mathrm{T}}\right)-\varepsilon_k\nabla p+\mathbf{M}_{kl}+\rho_k\varepsilon_k\mathbf{g} \tag{2}$$

where, ρ_k, $\mathbf{u}_k$, and ε_k represent, respectively, the macroscopic density, velocity, and volume fraction of phase k. $\mu_{k,eff}$ is the effective viscosity of the fluid phase k, including the molecular and turbulent contributions, p is the pressure, $\mathbf{M}_{kl}$, the interphase momentum exchange between phase k and phase l and $\mathbf{g}$ is the gravitational acceleration.

The momentum exchange between the gas (subscript G) and liquid phase (subscript L) phases is given by

$$\mathbf{M}_{L,G}=\frac{3}{4}\rho_L\frac{\varepsilon_G}{d_b}C_D\left(\mathbf{u}_G-\mathbf{u}_L\right)\left|\mathbf{u}_G-\mathbf{u}_L\right| \tag{3}$$

We have only included the drag force contribution to $\mathbf{M}_{L,G}$, in keeping with the works of Sanyal *et al.* [12] and Sokolichin and Eigenberger [13]. The added mass and lift forces have been ignored in the present analysis.

The interphase drag coefficient is calculated from [23]:

$$C_D=\frac{2}{3}\sqrt{\mathrm{E\ddot{o}}} \tag{4}$$

where the Eötvös number is defined as:

$$\mathrm{E\ddot{o}}=\frac{g(\rho_\mathrm{L}-\rho_\mathrm{G})d_\mathrm{b}^2}{\sigma} \tag{5}$$

where d_b is the equivalent diameter of the bubbles. The bubble diameter is taken to be 0.005 m, a typical value for air-water systems operating in the homogeneous bubbly flow regime.

For the continuous, liquid phase the turbulent contribution to the stress tensor is evaluated by means of the k-ε model, using standard single-phase parameters C_μ = 0.09, $C_{1\varepsilon}$ = 1.44, $C_{2\varepsilon}$ = 1.92, σ_k = 1, and σ_ε = 1.3. The applicability of the k-ε model has been considered in detail by Sokolichin and Eigenberger [13]. No turbulence model is used for calculating the velocity fields of the dispersed gas bubbles.

A commercial CFD package CFX version 4.4 of ANSYS Inc., Canonsburg, USA, was used to solve the equations of continuity and momentum. This package is a finite volume solver using body-fitted grids. The grids are non-staggered and all variables are evaluated at the cell centres. An improved version of the Rhie-Chow algorithm [24] is used to calculate the velocity at the cell faces. The pressure-velocity coupling is obtained using the SIMPLEC algorithm [25]. For the convective terms in Eqs. (1) and (2), hybrid differencing was used. A fully implicit backward differencing scheme was used for the time integration.

At the inlet patch, superficial liquid velocity U_{L0} and superficial gas velocity U_{G0} were maintained by setting the liquid holdup to $\varepsilon_{L0} = U_{L0}/(U_{G0}+U_{L0})$ the gas holdup to

1) List of symbols at the end of the paper.

ε_{G0} = 1-ε_{L0}, and the velocities of both phases to $\mathbf{u}_{G,z} = \mathbf{u}_{L,z} = (U_{L0}+U_{G0})$. At the outlet at the top, the gas holdup was set to $\varepsilon_{G,\mathrm{top}}$, and the liquid holdup to 1- $\varepsilon_{G,\mathrm{top}}$. The outlet velocities were specified as $\mathbf{u}_{G,z} = U_G/\varepsilon_{G,\mathrm{top}}$ and $\mathbf{u}_{L,z} = U_L/(1\text{-}\varepsilon_{G,\mathrm{top}})$. The gas holdup at the outlet patch at the top was chosen to be 5 %. It was verified that the gas holdup at the top had negligible influence on the results. The holdup and velocities near the top are adjusted to equilibrium values in a very short distance from the top, having little effect on the system average values. The gas and liquid phase were injected uniformly over the inner 80 % of the bottom patch. At the walls, no-slip boundary conditions were applied.

The time stepping strategy used in all simulations was 100 steps at $5{\cdot}10^{-5}$ s, 100 steps at $1{\cdot}10^{-4}$ s, 100 steps at $5{\cdot}10^{-4}$ s, 100 steps at $1{\cdot}10^{-3}$ s, 200 steps at $3{\cdot}10^{-3}$ s, 1400 steps at $5{\cdot}10^{-3}$ s, and the remaining steps until quasi-steady state is achieved at $1{\cdot}10^{-2}$ s. For each run, the hydrodynamics were solved first in a transient manner until quasi- steady state was reached. During the transient simulations the liquid sloshes from side to side in a chaotic manner, as can be evidenced in the animations on our website: http://ct-cr4.chem.uva.nl/contraction/.

Typical transient values of the centre line velocity $V_L(0)$ are shown in Fig. 2a for the 50 % inerts case.

2.2 CFD Modeling of A → B Reaction

The reaction run was initiated 10000 time steps after start of the hydrodynamic run. The following component balance equations are solved for the transferring component A in the gas phase:

$$\frac{\partial}{\partial t}\varepsilon_{\mathrm{G}}\rho_{\mathrm{G}}c_{\mathrm{AG}} + \nabla\cdot\left(\varepsilon_G\rho_G\mathbf{u}_{\mathrm{G}}c_{\mathrm{AG}} - \mathcal{D}_{\mathrm{G}}\varepsilon_{\mathrm{GL}}\rho_G\nabla c_{\mathrm{AG}}\right) = -\rho_{\mathrm{G}}F_{\mathrm{A}} \quad (6)$$

and liquid phase, respectively:

$$\frac{\partial}{\partial t}\varepsilon_{\mathrm{L}}\rho_{\mathrm{L}}c_{\mathrm{AL}} + \nabla\cdot\left(\varepsilon_{\mathrm{L}}\rho_{\mathrm{L}}\mathbf{u}_{\mathrm{L}}c_{\mathrm{AL}} - \mathcal{D}_{\mathrm{L}}\varepsilon_{\mathrm{L}}\rho_{\mathrm{L}}\nabla c_{\mathrm{AL}}\right) = \rho_{\mathrm{AL}}(F_{\mathrm{A}} + \varepsilon_{\mathrm{L}}r_{\mathrm{A}}) \quad (7)$$

Here, c_{AL} is the concentration of component A in the liquid phase, $\mathcal{D}_L$ is the diffusion coefficient of component A. The consumption due to the reaction of component A is denoted by r_{A}. The flux F_{A} is the interphase transfer flux of A between the gas and liquid phases:

$$F_A = k_L a(mc_{AG} - c_{AL}) \quad (8)$$

where k_L is the mass transfer coefficient and m is the Henry coefficient. The mass transfer coefficient k_L was chosen as $4{\cdot}10^{-4}$ m/s. The Henry coefficient m was chosen as 0.3. The physical and transport properties of the components are specified in Tab. 1. The specific interfacial a per unit volume of reactor (gas+liquid) is calculated from:

$$a = \frac{6\varepsilon_G}{d_b} \quad (9)$$

With gas contraction, the mass continuity equation Eq. (1) needs modification to reflect the disappearance of the component A from the gas phase using the sink term F_{A}. No flux of component A is allowed through the walls. To ensure that no flux of the component takes place across the flow boundaries with zero ingoing flow, the boundary value for the mass component concentration is set equal to the value inside the computational domain at each iteration for these boundaries.

At the start of the reaction run, the gas inlet concentration of A, c_{AG0}, makes a step from zero to values of 0.9, 0.7, 0.5, and 0.1 arbitrary units per m^3 for the simulations with 10 %, 30 %, 50 %, and 90 % inerts, respectively. The inflowing liq-

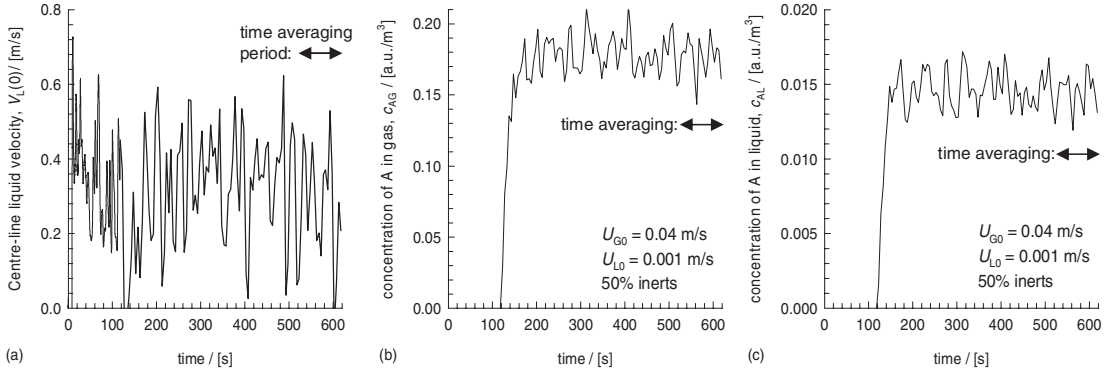

Figure 2. Transient approach to quasi-steady state for (a) centerline liquid velocity $V_L(0)$, (b) concentration of A in gas phase, (c) concentration of A in liquid phase. The simulation results correspond to the case for U_{G0} = 0.04 m/s, U_{L0} = 0.001 m/s and 50 % inerts in inlet gas stream. The values correspond to a position 4.5 m above the bottom at the centre of the column. Typical animations are to be found on our website: http://ct-cr4.chem.uva.nl/contraction/.

uid stream does not contain any component A. The gas inlet concentration c_{BG} and the liquid inlet concentrations c_{AL} and c_{BL} remain zero at all times. Component A transfers from the gas to the liquid phase and in the liquid phase, component A reacts to component B. Component B is considered to be present only in the liquid phase.

The reaction term in Eq. (7) is:

$$r_A = -k_A C_{AL} \tag{10}$$

We assume $k_A = 0.2\ s^{-1}$ ensuring a mass transfer limited situation.

For the 3D simulations, Eqs. (1), (2), (6), and (7) need to be solved simultaneously until the system attains quasi-steady state with respect to concentrations. Time steps of 0.1 s were taken, until the component concentrations in the system attained (quasi-) steady state; typical transience of the gas and liquid phase concentrations are shown in Fig. 2b,c for the case with 50 % inerts. Time averaging over the quasi-steady state period is required in order to determine the reactor performance. The time-averaging period is indicated by the double-headed arrows in Fig. 2.

Further details of the numerical techniques used in our CFD simulations, including animations, are to be found on our website: http://ct-cr4.chem.uva.nl/contraction/.

3 Simulation results

Cross-sectional area averaging of the time-averaged values yields the profiles along the height of the reactor. Let us first consider the variation of (a) superficial gas velocity, U_G, and (b) gas holdup, ε_G along the height of the reactor; see Figs. 3a and b. We note that as a consequence of the disappearance of A from the gas phase due to the mass transfer, and subsequent chemical reaction, U_G decreases along the reactor height. This reduction in U_G is larger when the inerts content in the incoming gas stream is lower. For the 10 % inerts case we note that the value of U_G decreases from 0.04 m/s at the reactor inlet to a value of 0.014 m/s at the reactor outlet. The reduction in the gas velocity with decreasing inerts content has a significant effect on the gas holdup; see profiles in Fig. 3b. Averaging the gas holdup over all grid cells in the computational domain yields the gas holdup values reported in Fig. 3c. With decreasing inerts content, there is a significant reduction in the *average* gas holdup and as a consequence there is a reduction in the interfacial area according to Eq. (9).

Concentration profiles for A in the gas and liquid phases along the column height under quasi-steady state conditions, obtained after cross-sectional area averaging, are shown in Figs. 4a and b. For the 90 % and 50 % inerts cases, the c_{AG}

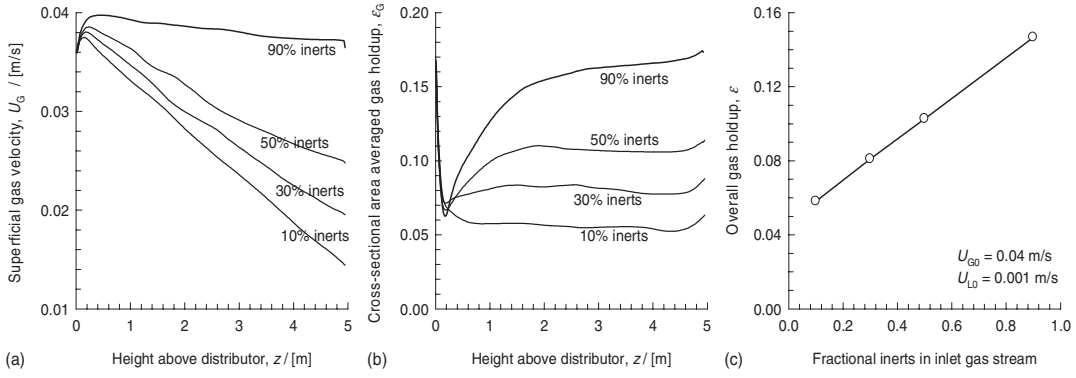

Figure 3. Profiles along the reactor height (time averaged over the time period wherein quasi-steady state prevails) of (a) superficial gas velocity, and (b) gas holdup. (c) Average gas holdup in the reactor as a function of the fractional inerts content of the inlet gas stream. In all simulation campaigns U_{G0} = 0.04 m/s, U_{L0} = 0.001 m/s and with varying % inerts in inlet gas stream.

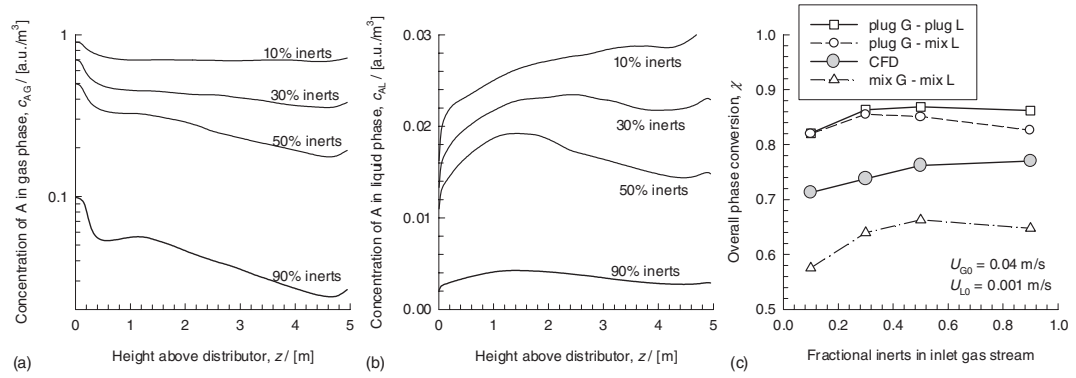

Figure 4. Profiles along the reactor height (time averaged over the time period wherein quasi-steady state prevails) of (a) gas phase concentration, (b) liquid phase concentration. (c) Conversion of A as a function of the fractional inerts content of the inlet gas stream. In all simulation campaigns U_{G0} = 0.04 m/s, U_{L0} = 0.001 m/s and with varying % inerts in inlet gas stream.

profile appears to follow a steady decrease expected of the situation in which we have a plug flow of the gas phase. With further decrease in the inerts content, the gas phase concentration profiles tend to flatten out after the initial decrease in the gas concentration that occurs within the first 1 m of reactor height. Examination of the liquid phase concentration profiles shows that the variation with the reactor height is very small for all cases, indicating that the liquid phase concentration profiles tend to approximate the well-mixed liquid scenario.

The overall reactor conversion χ of A increases with increasing inerts fraction in the inlet gas stream; see Fig. 4c. An important reason for this is the increase in gas holdup with increasing inerts fraction as witnessed in Fig. 3c. A higher gas holdup leads to a higher interfacial area that is advantageous for mass transfer limited reactions, as is the situation here for the chosen set of parameters.

To gain further insights into the results presented in Fig. 4c we carried out calculations for concentration profiles and conversion using conventional bubble column reactor models as discussed, for example, by Deckwer [4]. Three special scenarios can be identified:

(I) Plug flow of gas and plug flow of liquid,
(II) Plug flow of gas and well mixed liquid, and
(III) well mixed gas and well-mixed liquid.

Consider scenario (I) for which the differential equations describing the variation of c_{AG} and c_{AL} are

$$\frac{d(U_G c_{AG})}{dz} = -k_L a(mc_{AG} - c_{AL}) \tag{11}$$

and

$$U_L \frac{dc_{AL}}{dz} = k_L a(mc_{AG} - c_{AL}) - (1-\varepsilon_G)k_A c_{AL} \tag{12}$$

where the variables c_{AG}, c_{AL}, and U_G are z-dependent. The superficial liquid velocity does not alter significantly as a result of chemical reaction. At any position along the height, c_{AG} is given by the relation:

$$c_{AG} = c_{AG0}\left(\frac{U_G - U_{GI}}{U_{G0} - U_{GI}}\right) \tag{13}$$

For scenario (II), the liquid phase is assumed to be well mixed; therefore, c_{AL} is z-invariant and corresponds to the value at the reactor outlet and can be obtained from a material balance

$$c_{AL} = \frac{\int_{z=0}^{H_T} k_L a(mc_{AG} - c_{AL})dz - (1-\varepsilon)k_A C_{AL} H_T}{U_L} \tag{14}$$

For the case in which the gas phase and liquid phases are both well-mixed (scenario (III)), both c_{AG} and c_{AL} within the reactor are z-invariant and are given by:

$$c_{AG} = \frac{U_{G0}c_{AG0} - k_L a(mc_{AG} - c_{AL})H_T}{U_{G0}C_{AG} + U_{GI}} \tag{15}$$

and

$$c_{AL} = \frac{k_L a(mc_{AG} - c_{AL})H_T - (1-\varepsilon)k_A c_{AL} H_T}{U_L} \tag{16}$$

For all three scenarios, the reactor equations were solved numerically to obtain the concentration profiles and conversion. In the calculations for the three scenarios, we used the *average* gas holdup as determined from CFD simulations and reported in Fig. 3c. In Fig. 5a, the calculations of the three scenarios for c_{AG} profiles are compared with the CFD solutions for the 90 % inerts case. Except for the initial zone at the bottom of the reactor, there is reasonably good agreement between the plug flow profiles (scenarios (I) and (II)) and the CFD simulations. The corresponding results for c_{AL} are shown in Fig. 5b. The CFD simulation results for the liquid concentration profiles are in closer agreement with the

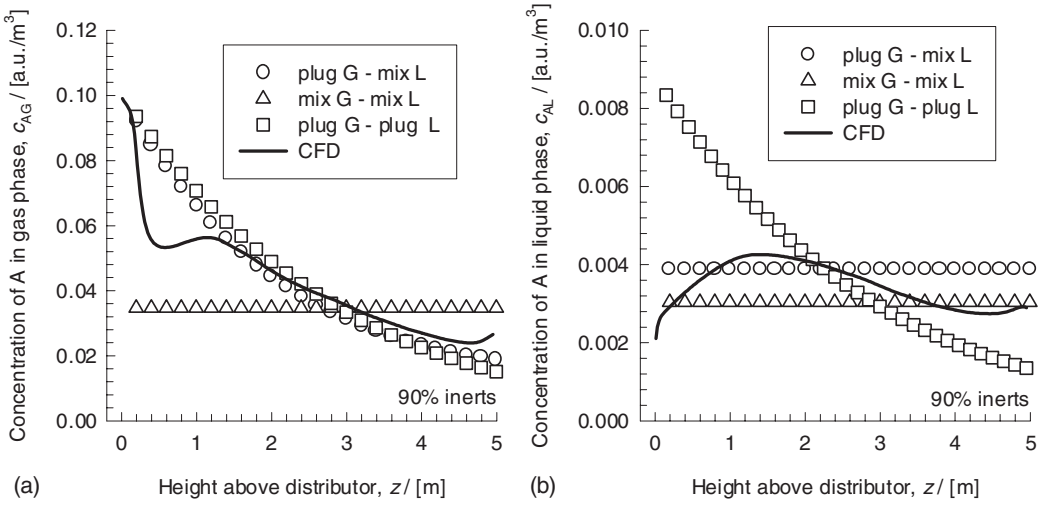

Figure 5. Profiles along the reactor height (time averaged over the time period wherein quasi-steady state prevails) of (a) gas phase concentration, and (b) liquid phase concentration for the 90 % inerts case. The CFD simulations (continuous solid lines) are compared with profile calculations for three special scenarios: (I) plug flow of gas and liquid (II) gas phase in plug flow and well-mixed liquid phase, and (III) well mixed gas and liquid phases.

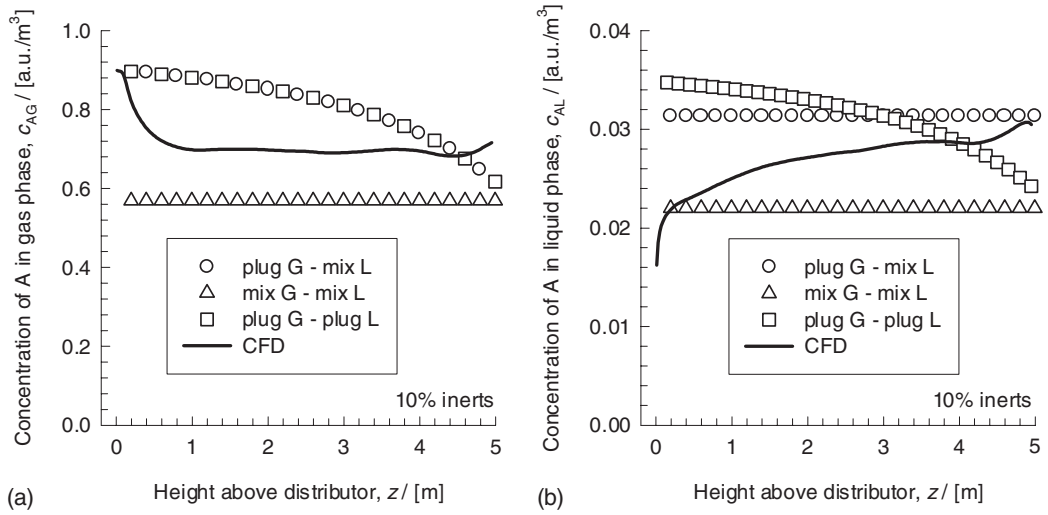

Figure 6. Profiles along the reactor height (time averaged over the time period wherein quasi-steady state prevails) of (a) gas phase concentration, (b) liquid phase concentration for the 10 % inerts case. The CFD simulations (continuous solid lines) are compared with profile calculations for three special scenarios: (I) plug flow of gas and liquid (II) gas phase in plug flow and well-mixed liquid phase, and (III) well mixed gas and liquid phases.

well-mixed assumption (scenarios (II) and (III)) than with the assumption of the plug flow of liquid (scenario (I)).

When the inerts concentration is lowered, the situation is changed significantly, as is evidenced by the profiles shown in Fig. 6 for the 10 % inerts case. The gas phase concentration profiles (see Fig. 6a) lie in between those predicted by the plug flow and well mixed assumptions. Note that the two plug flow scenarios (I) and (II) yield profiles that are indistinguishable from each other. The liquid phase concentration profiles (see Fig. 6b) do not appear to conform to any of the three scenarios.

The overall conversions predicted by the three scenarios are compared with the CFD simulation results in Fig. 4c. The CFD simulation results for the conversion lie in between the conversions predicted by model scenarios (II) and (III). The assumption of plug flow of gas becomes progressively worse when the inerts content is decreased.

4 Conclusions

In this paper we have developed a CFD model for describing a bubble column reactor for carrying out a first order liquid phase reaction A → B including the influence of gas contraction. The bubble column reactor is assumed to operate in the homogeneous bubbly flow regime. When the incoming gas contains a high proportion of inerts, the reactor performance can be well approximated by model (II) (plug flow of *G* and well mixed *L*). When the inerts content decreases, the assumption of the plug flow of gas becomes increasingly worse and the conversion predictions are too optimistic. The predictions of model (III) (well mixed *G* and well mixed *L*) is too pessimistic in all cases. The computational results obtained in this paper demonstrate the power of CFD for accurately predicting the performance of bubble column reactors. Simplified reactor models, as discussed by Deckwer [4] yield either too optimistic or too pessimistic results.

Acknowledgement

The Netherlands Organisation for Scientific Research (NOW-CW) is gratefully acknowledged for providing financial assistance in the form of a Programmasubsidie for development of *novel concepts in reactive separations* and also a TOP subsidie for Intensification of Reactors.

Received: July 16, 2004 [CET 7018]

Nomenclature

a	[m^{2}m^{-3}]	interfacial area per unit volume of dispersion
C_D	[–]	drag coefficient
c_{AG}	[a.u.m^{-3}]	gas phase concentration
c_{AL}	[a.u.m^{-3}]	liquid phase concentration
d_b	[m]	diameter of bubble
$Đ$	[m^2 s^{-1}]	diffusivity
D_T	[m]	column diameter
Eö	[–]	Eötvös number, $g(\rho_L - \rho_G)d_b^2/\sigma$
F	[a.u.s^{-1}]	interfacial mass transfer rate
$\boldsymbol{g}$	[m s^{-2}]	gravitational vector
H_T	[m]	total height of reactor
k_A	[s^{-1}]	first order reaction rate constant defined in Eq. (10)
k_L	[m/s]	mass transfer coefficient in liquid phase
m	[–]	Henry coefficient
$\mathbf{M}$	[N/m^3]	interphase momentum exchange term
p	[Pa]	pressure
r_A	[a.u.s^{-1}]	reaction rate of component A

t	[s]	time
u	[m/s]	velocity vector
U_G	[m s^{-1}]	superficial gas velocity
U_L	[m s^{-1}]	superficial liquid velocity
$V_L(0)$	[m s^{-1}]	centre-line liquid velocity
z	[m]	height above the distributor at bottom of reactor

Greek

χ	[–]	conversion
ε	[–]	gas holdup
μ	[Pa s]	viscosity of fluid phase
ρ	[kg m^{-3}]	density of phase
σ	[N m^{-1}]	surface tension of liquid phase

Subscripts

0	at reactor inlet
A	referring to component A
b	referring to bubbles
eff	effective
G	referring to gas
in	referring to inlet to reactor
I	referring to inerts
k	referring to phase k
l	referring to phase l, $l \neq k$
L	referring to liquid
out	referring to outlet of reactor
top	referring to the top of the column
T	tower or column
z	in vertical (axial) direction

References

[1] C. Maretto, R. Krishna, *Catal. Today* **1999**, *52*, 279.
[2] S. T. Sie, R. Krishna, *Appl. Catal., A* **1999**, *186*, 55.
[3] R. Krishna, S. T. Sie, *Fuel Process Technol.* **2000**, *64*, 73.
[4] W. D. Deckwer, *Bubble Column Reactors*, John Wiley, New York, NY **1992**.
[5] A. Forret, J.-M. Schweitzer, T. Gauthier, R. Krishna, D. Schweich, *Chem. Eng. Sci.* **2003**, *58*, 719.
[6] C. O. Vandu, R. Krishna, *Chem. Eng. Technol.* **2003**, *26*, 779.
[7] C. O. Vandu, R. Krishna, *Chem. Eng. Process.* **2004**, *43*, 575.
[8] C. O. Vandu, R. Krishna, *Chem. Eng. Process.* **2004**, *43*, 987.
[9] H. A. Jakobsen, B. H. Sannaes, S. Grevskott, H. F. Svendsen, *Ind. Eng. Chem. Res.* **1997**, *36*, 4050.
[10] J. B. Joshi, *Chem. Eng. Sci.* **2001**, *56*, 5893.
[11] Y. Pan, M. P. Dudukovic, M. Chang, *Chem. Eng. Sci.* **1999**, *54*, 2481.
[12] J. Sanyal, S. Vasquez, S. Roy, M. P. Dudukovic, *Chem. Eng. Sci.* **1999**, *54*, 5071.
[13] A. Sokolichin, G. Eigenberger, *Chem. Eng. Sci.* **1999**, *54*, 2273.
[14] R. Krishna, J. M. van Baten, *Chem. Eng. Res. Des.* **2001**, *79*, 283.
[15] R. Krishna, J. M. van Baten, M. I. Urseanu, *Chem. Eng. Technol.* **2001**, *24*, 451.
[16] R. Krishna, J. M. van Baten, *Catal. Today* **2003**, *79*, 67.
[17] R. Krishna, J. M. van Baten, *Chem. Eng. Technol.* **2002**, *25*, 1015.
[18] R. Krishna, J. M. van Baten, M. I. Urseanu, *Chem. Eng. Sci.* **2000**, *55*, 3275.
[19] R. Krishna, M. I. Urseanu, J. M. van Baten, J. Ellenberger, *Chem. Eng. Sci.* **1999**, *54*, 4903.
[20] J. M. van Baten, R. Krishna, *Chem. Eng. Res. Des.* **2004**, *82*, 1043.
[21] J. M. van Baten, R. Krishna, *Ind. Eng. Chem. Res.* **2004**, *43*, 4483.
[22] J. M. van Baten, R. Krishna, *Chem Eng Technol*. **2004**, *27*, 398.
[23] R. Clift, J. R. Grace, M. E. Weber, *Bubbles, Props and Particles*, Academic Press, San Diego, CA **1978**.
[24] C. M. Rhie, W. L. Chow, *A.I.A.A.J.* **1983**, *21*, 1525.
[25] J. van Doormal, G. D. Raithby, *Numer. Heat Transfer* **1984**, *7*, 147.

